Chalcogenide Letters Vol. 19, No. 7, July 2022, p. 483 - 492

Structural, optical, and electrical properties of chemically sprayed Cu_2MnSnS_4 thin films

A. J. Salh, N. A. Bakr*
Department of Physics, College of Science, University of Diyala, Iraq

In this paper, Cu_2MnSnS_4 (CMTS) thin films are prepared by chemical spray pyrolysis on glass substrates at a temperature of (400 ± 10°C), using 0.04 M of copper chloride, 0.02 M of manganese chloride, 0.02 M of tin chloride and different concentrations of thiourea (0.14, 0.16, 0.18, 0.20, 0.22, and 0.24 M) as source precursors. XRD diffraction, Raman spectroscopy, FESEM, UV-Vis spectroscopy, and the Hall effect technique were used to examine the structural, morphological, optical, and electrical properties. The results of XRD diffraction show that all films are polycrystalline in nature with tetragonal structure stannite structure. The maximum crystallite size of the CMTS thin films was determined using Scherrer's formula, and it was found to be (12 nm) at (0.20 M) thiourea concentration. The main peak of the Raman spectroscopy data is located at 327 cm^{-1}, which is attributed to the vibration mode originating from the sulfur sub lattice vibration. In the wavelength range of (300-900) nm, optical characteristics such as absorbance and transmittance spectra were measured. With a high absorption coefficient (10^4 cm^{-1}), the optical energy band gap of the prepared films ranges hand, electrical tests through the Hall effect of CMTS thin films show that they have an electrical conductivity of p-type.

(Received March 17, 2022; Accepted July 22, 2022)

Keywords: Cu_2MnSnS_4 thin films, Chemical spray pyrolysis, Concentration of thiourea, Structural properties, Optical properties, Hall effect

1. Introduction

I_2-II-IV-VI_4 quaternary chalcogenides have been actively explored in recent years as potential light-absorbing possibilities for solar cells [1]. Because of their optimum metal richness in the earth's crust and a direct band gap [2,3], during the last few years, copper-based quaternary chalcogenide semiconductors have gotten a lot of attention as low-cost alternatives to traditional absorber materials in photovoltaics. Cu_2MnSnS_4 (CMTS) can be one of the viable light absorber materials in the search for additional Cu-based quaternary chalcogenide semiconductor options since it is plentiful and nontoxic ingredients, good absorption coefficient and large absorption coefficient (1.1 eV - 1.3 eV) straight band gap [4-6]. The naturally occurring mineral CMTS encapsulates in a stannite structure (space group: I 42 m) that resembles kieserite CZTS structurally (space group: I 4). These compounds have received a lot of attention recently since they are cheap, non-toxic, common on the planet, and have a high absorption coefficient [7]. Copper chalcogenides are well suited for a variety of applications, including photovoltaic, ultra-capacitors, memory chips, and light-emitting diodes [8, 9]. Thermal evaporation [10], sol-gel [11], chemical vapor deposition [12], and electro deposition technique [13] are some of the techniques that have been used to deposit thin coatings of copper manganese tin sulfide where the Cu_2MnSnS_4 (CMTS) thin films are researched and addressed in terms of structural, elemental analysis, optical, and electrical properties.

* Corresponding author: nabeelalibakr@yahoo.com
https://doi.org/10.15251/CL.2022.197.483

2. Experimental Method

In this study, Cu_2MnSnS_4 thin films are deposited on glass substrates at (400 ± 10 °C) using chemical spray pyrolysis (CSP) technique. The glass slides were cut and after that they were ultrasonically rinsed with distilled water, ethanol, and distilled water for ten minutes each time, before being dried with soft paper. Spray solution was prepared by dissolving 0.04 M of copper chloride dihydrate ($CuCl_2.2H_2O$), 0.02 M of manganese chloride ($MnCl_2.4H_2O$), 0.02 M of tin chloride dehydrate ($SnCl_2.2H_2O$) and different concentrations of thiourea ($SC(NH_2)_2$) as shown in table (1). The powders were weighed using a sensitive electronic balance (Mettler AE-160 type) with sensitivity of (10^{-4} g) and dissolved separately in 25 ml of distilled water. The final volume of 100 mL was achieved by stirring the four solutions together with a magnetic stirrer for half an hour to ensure homogeneity and purity. After that, this solution was sprayed on glass substrates for 10 seconds before being stopped for 1 minute to guarantee that the reaction occurs and to allow the film layer to grow, as well as to maintain the substrate temperature at 400 °C. The spraying procedure was repeated until the desired film thickness (350 ±10 nm) was achieved. All other parameters, such as the size of the nozzle through which the material is discharged, the carrier gas pressure (1.5 bar), and the distance between the nozzle and the glass substrate (30 cm), remained constant throughout the deposition process for all samples. The resulting films were stable and consistent in appearance, with good adhesive qualities. The gravimetric method was used to determine the thickness of the deposited films using the following relationship:

$$t = \frac{\Delta m}{\rho \, . \, s} \tag{1}$$

Where t is the thickness of the thin film, Δm is the weight difference between the clean substrate and the substrate after deposition, ρ is the compound density, and s is the area of substrate.

Table 1.Thiourea molar concentrations used in CMTS films preparation.

Sample code	$SC(NH_2)_2$ concentration (M)
CMTS1	0.14
CMTS2	0.16
CMTS3	0.18
CMTS4	0.20
CMTS5	0.22
CMTS6	0.24

3. Results and Discussion

3.1. XRD Analysis

Fig.1 shows the X-ray diffraction patterns of CMTS films, The diffraction patterns were studied using an X-ray generator where the X-ray diffraction peaks appeared at (2Θ~28.21°, 32.44˚, 46.99˚, 55.30˚, and 75.81˚), in accordance with the planes (112), (200) , (204), (312), and (316) respectively with a dominant and favorable direction of growth (112) for all films these results are somewhat consistent with the standard card (ICDD) serial number (00-051-0757) . The space group of CMTS crystallizes in a tetragonal stannite structure (I 42 m) because the CMTS is a quaternary compound [7] with a conventional tetragonal structure containing sixteen atoms, secondary phase crystallization is conceivable (4 copper, 2 manganese, 2 tin, 8 sulfur atoms). As MnSn/SS/CuCu/SS, the order in the cation sublattice of the metal ions can be achieved by

alternating along the crystalline c-direction, cation layers with sulfur anion layers. The lattice vector is the ratio (c/2a), which is less than 1 for all samples as shown in table 2, indicating that the lattice is compressed in the c-axis direction [14]. The interplanar distance (d) of the tetragonal structure is given by [15]:

$$\frac{1}{d^2} = \left(\frac{h^2 + k^2}{a^2}\right) + \frac{l^2}{c^2} \tag{2}$$

where the Miller indices are expressed by h, k, and ℓ, and the lattice constants are represented by a and c. The constants of the standard lattice (a = b = 5.5136 Å and c = 10.8260 Å) are close to the values depicted in table (2). The crystallite size of the deposited CMTS thin film is determined using Scherrer's formula, as illustrated in the following equation [16]:

$$D = \frac{k\lambda}{\beta cos\theta} \tag{3}$$

where β is the full width half maxima of the main peak measured in radians, λ is the wavelength of X-ray incident on the target with the value of 1.54056 Å, and K the shape factor taken to be 0.9.

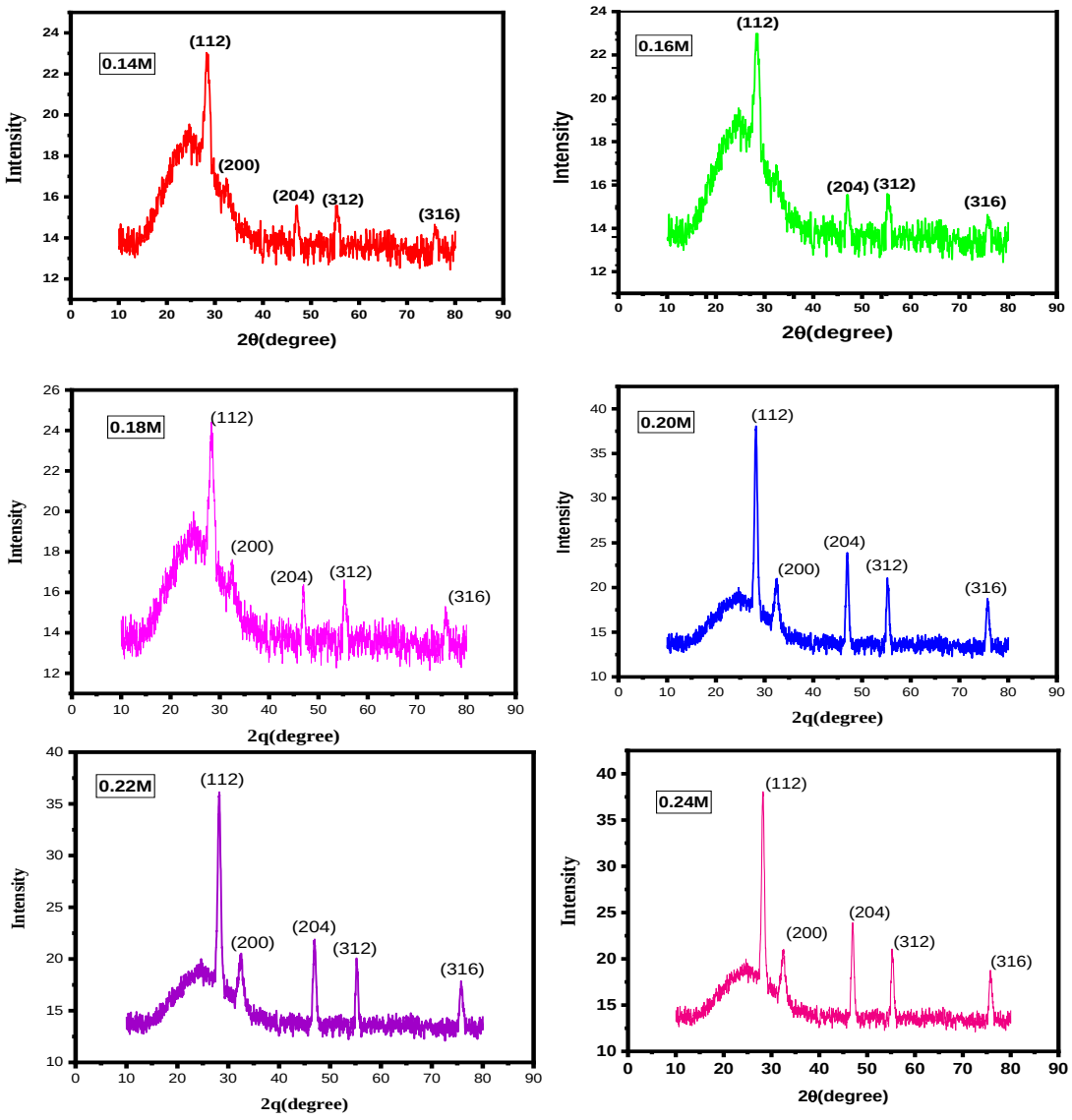

Fig. 1. X-ray diffraction patterns of CMTS thin films at different concentrations of thiourea.

Table 2. Structural parameters of the XRD results of (CMTS) thin films at different concentrations of thiourea.

Sample code	Concentrations of thiourea (M)	2θ (deg.)	β (rad.)	d (Å)	D (nm)	Lattice constants (Å)		c/2a	Unit cell volume ($Å^3$)
						a = b	c		
CMTS1	0.14	28.45	0.0206	3.149	6.935	5.5422	10.819	0.981	332.31
CMTS2	0.16	28.42	0.0205	3.122	6.963	5.507	10.830	0.977	328.44
CMTS3	0.18	28.31	0.0184	3.158	7.735	5.5220	10.820	0.997	329.93
CMTS4	0.20	28.215	0.0119	3.160	12.00	5.5133	10.821	0.983	328.90
CMTS5	0.22	28.21	0.0123	3.157	11.60	5.4656	10.860	0.980	324.41
CMTS6	0.24	28.1	0.0164	3.734	8.18	5.4580	10.630	0.9813	316.66

3.2. Raman Spectrometer Analysis

The Raman shift is used to identify whether a substance contains secondary phase or not. Table (3) shows the analysis of the Raman spectra of the deposited samples which are shown in fig.2. It can be seen that all samples have similar Raman signals, with a high peak at ~ 327cm^{-1}, which is commonly credited to the vibrational mode originating from the sulfur sublattice vibration [17], and smaller contributions at ~ 245 and ~ 344 cm^{-1} [18, 19]. This demonstrates the absence of any impurity phases and validates the presence of the CMTS phase [17].

Table 3. Results of Raman spectroscopy of CMTS thin films at different concentrations of thiourea.

Concentrations of thiourea (M)	Peak center (cm^{-1})	Peak width (cm^{-1})	Peak Intensity (arb. u.)
0.14	245.35	10.59	2.80
	326.95	11.92	70.8
	344.56	9.59	4.09
0.16	244.50	7.66	4.10
	326.98	10.02	72.86
	344.16	7.86	4.78
0.18	244.19	6.50	5.08
	327.04	7.98	75.57
	343.47	7.54	5.13
0.20	243.38	5.75	5.92
	327.01	3.01	69.68
	344.02	8.63	5.10
0.22	244.30	8.70	4.10
	327.04	10.46	73.26
	344.62	7.63	4.73
0.24	245.33	8.68	2.87
	326.94	11.96	70.63
	344.98	10.06	4.09

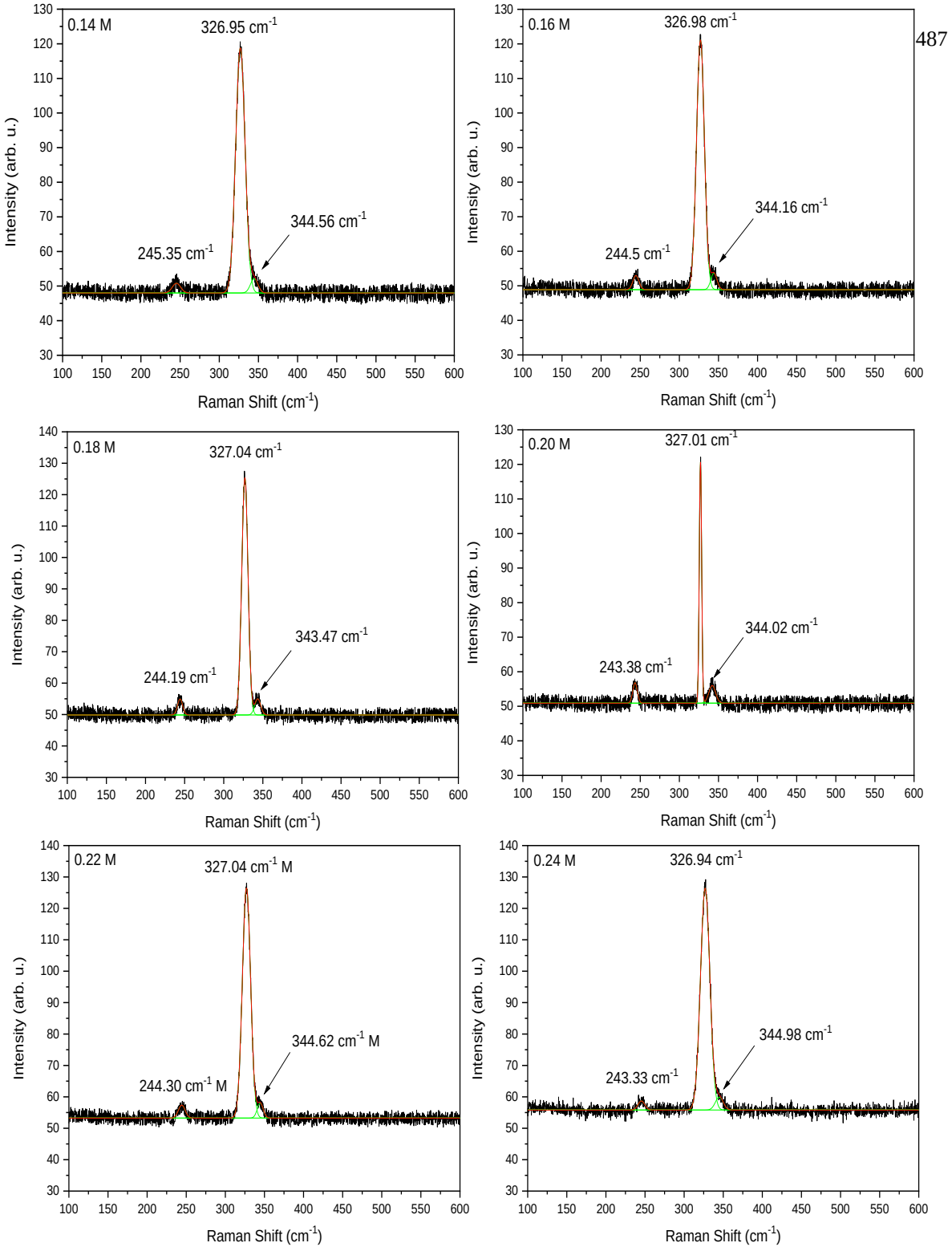

Fig. 2. Raman spectra of CMTS thin films different concentrations of thiourea.

3.4 Optical Properties

UV-visible 1800 spectrophotometer device equipped with a range of wavelengths (300-1100) nm from the Japanese manufacturer (Shimadzu) was used to measure the optical characteristics. This instrument measures transmittance and absorbance. The following equation can be used to compute the absorption coefficient:

$$\alpha = 2.3032\, A/t \tag{4}$$

where A is the absorbance, t is the thickness of the film, and α is the absorption coefficient. The α values obtained for all the films were > 10^4 cm^{-1} suggesting an allowed direct electronic transition. The optical allowed direct energy gap can be calculated by Tauc's formula [20]:

$$\alpha h\nu = P(h\nu - E_g)^r \quad (5)$$

where hν is the photon energy (eV), P is a constant depends on the nature of the film material, Eg is the optical energy gap, r is an exponential coefficient depending on the transition nature (r = 1/2 for allowed direct transition). The energy gap value of the thin films at the intersection point is calculated by plotting a graph between $(\alpha h\nu)^2$ and photon energy (hν) in (eV) and extrapolating the straight region of the plot to the x-axis at $(\alpha h\nu)^2 = 0$. The thin films studied have an energy gap between (1.88-1.96) eV. As the concentration of thiourea increases, the value of the energy gap increases as well. The increase in the energy gap is due to the decrease in the localized state between the valance and conduction bands.

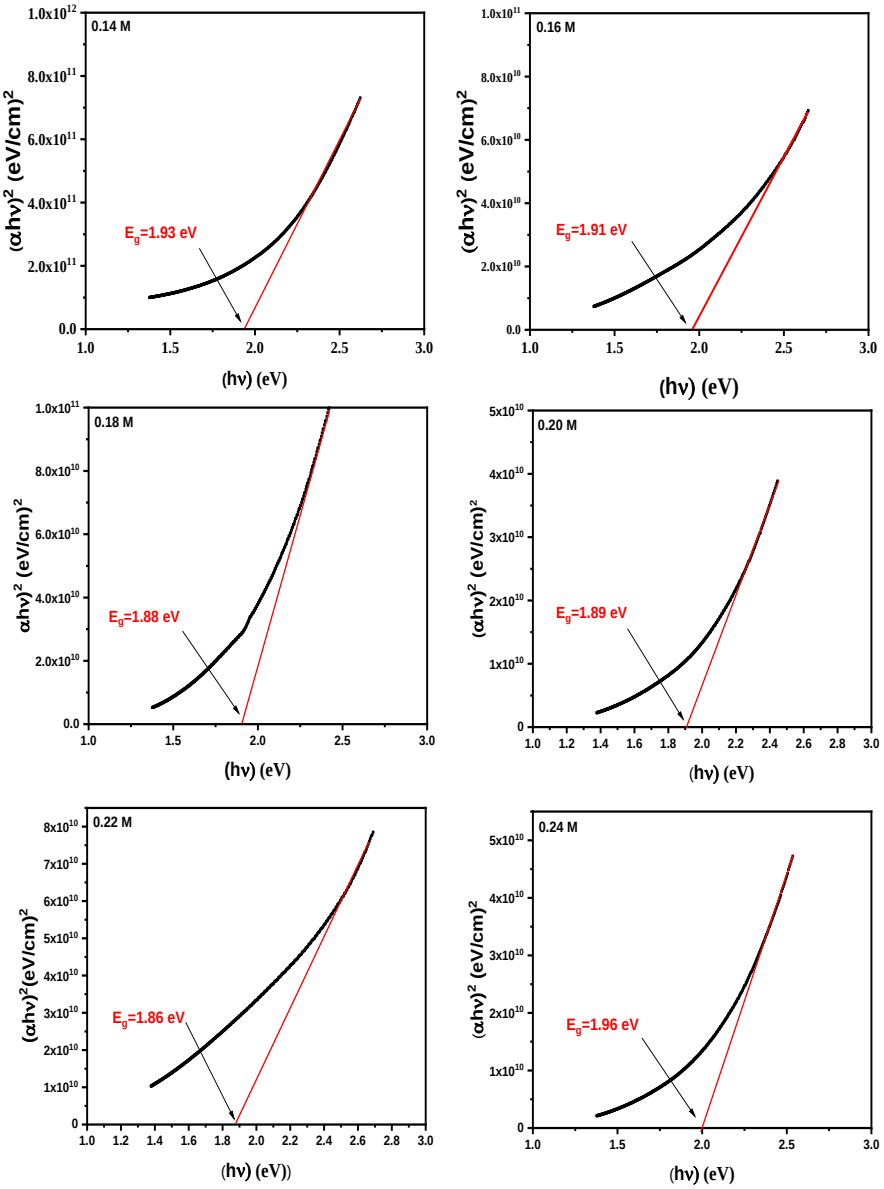

Fig 4. Tauc's plot of CMTS thin films at different concentrations of thiourea.

3.5. Scanning Electron Microscopy with Field Emission (FESEM) measurement

The nature of the thin films surface was investigated using the field emission electron microscopy (FESEM) technique. Micro graphics of (CMTS) thin films made with varying concentrations of thiourea at a temperature of 400°C are shown in Figure (5) with a magnification power of (50 KX). On the nanoscale, shapes like cauliflower can be seen. Some voids and gaps are observed as a result of secondary growth occurring at the surface prior to the previous layer's completion.

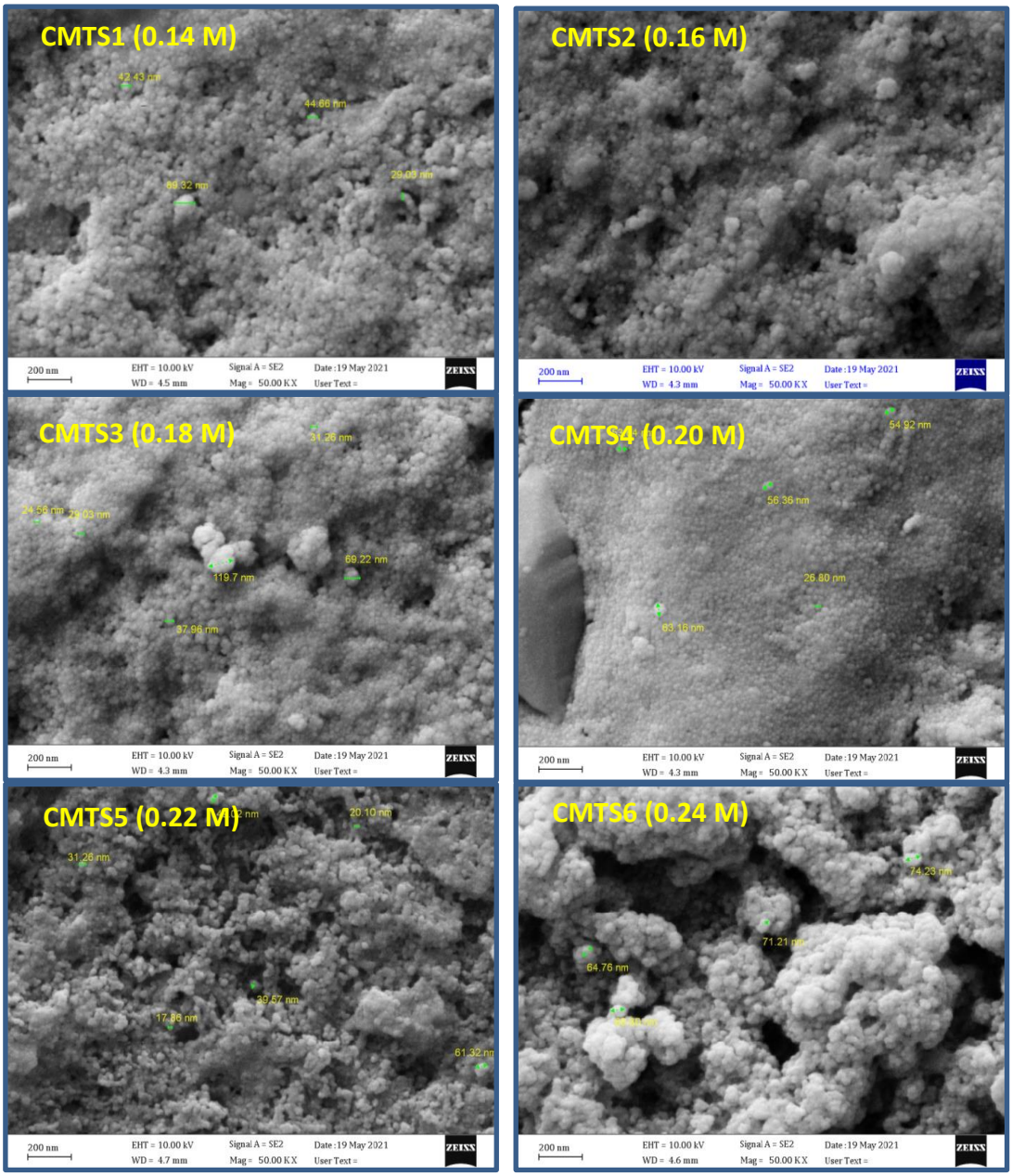

Fig. 5. FESEM micro of CMTS thin films at different concentrations of thiourea.

3.6. Electrical measurements

P-type conductivity was observed in Hall effect experiment conducted at ambient temperature (300 K) where Ecopia HMS-3000 device was used. The film CMTS4 has a high concentration of free holes ($\rho_{Hall} = 0.931\times10^{18}$ cm^{-3}) and a maximum conductivity value of (0.4938 $(cm)^{-1}$), as shown in figures (5) and (6), and depicted in table (4). It is noticed that the electrical

conductivity increases with increasing the concentration of thiourea, where it reaches its highest value at thiourea concentration of (0.2 M) for the CMTS4 thin film. Then it decreases due to the defects resulting from Mn and Sn in the films. These defects restrict the movement of electrons and increase their resistance, making them an (N-type) semiconductor.

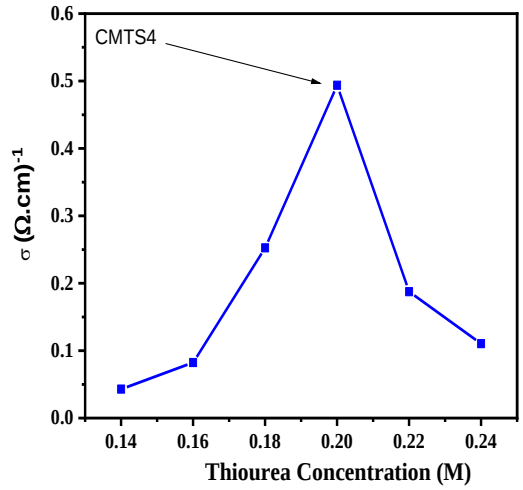

Fig. 5. Variation of Hall conductivity with thiourea concentration of CMTS thin films.

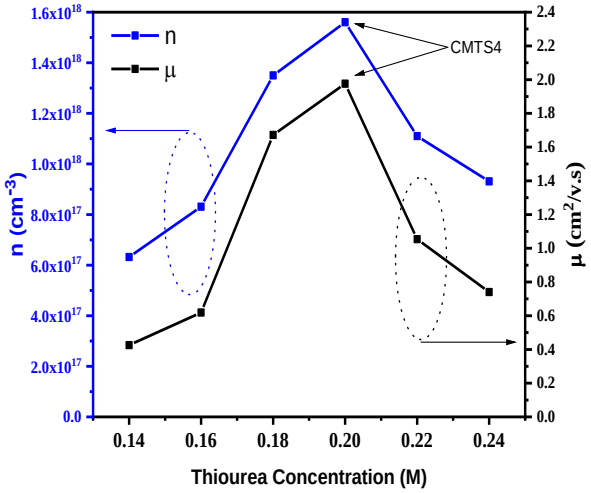

Fig. 6. Variation of charge carriers concentration and mobility with thiourea concentration for CMTS thin films.

Table 4. Results of the Hall effect experiment of CMTS thin films.

Sample code	R_H (cm^3/C)	n (cm^{-3}) ×10^{18}	μ (cm^2/V.s)	ρ (Ω.cm)	σ $(\Omega.cm)^{-1}$
CMTS1	9.8758	0.632	0.4254	23.2152	0.0430
CMTS2	7.5108	0.831	0.6188	12.1374	0.0823
CMTS3	4.6233	1.35	1.1672	3.9611	0.2524
CMTS4	4.001	1.56	1.9758	2.0250	0.4938
CMTS5	5.623	1.11	1.0541	5.3344	0.1874
CMTS6	6.7041	0.931	0.7406	9.0620	0.1103

4. Conclusions

Spray pyrolysis was used to deposit a thin film of Cu_2MnSnS_4 at temperature of (400±10) °C on glass substrates. The XRD diffraction results demonstrate that all film have a tetragonal stannite structure, with an estimated crystallite size (12.0 nm) for the sample deposited using thiourea concentration of 0.20 M. Raman spectra confirmed the XRD diffraction results, which exhibited a definite primary peak of high strength situated at (~327 cm^{-1}) with secondary peaks of lower intensity. As seen by the FESEM results on the nanoscale, cauliflower-like spherical and semi-spherical shapes can be seen. The optical test results show that CMTS thin films have an energy gap in the range of (1.88-1.96 eV) with a high coefficient of absorption, making them suitable for applications involving solar cells. Electrical investigations of CMTS thin films using the Hall effect reveal that they have p-type electrical conductivity, with increasing electrical conductivity with thiourea concentration reaching its highest value at a concentration of (0.20 M) for the CMTS4 thin film, which is consistent with XRD results.

References

[1] X. Chen, J. Liu, J. Feng, E. Zhang, H. Wang, X. Liu, J. Liu, H. Rong, M. Xu, J. Zhang, Journal of Materials Chemistry A,Vol.6, No.25, pp.1-12, (2018); https://doi.org/10.1039/C8TA03070G

[2] K. V. Gurav, S. W. Shin, U. M. Patil, M. P. Suryawanshi, S. M. Pawar, M. G. Gang, S. A. Vanalakar, J. H. Yun, J. H. Kim, Journal of Alloys and Compounds, Vol.631, pp 178-182, (2015); https://doi.org/10.1016/j.jallcom.2014.12.253

[3] K. Woo, K. Kim, Z. Zhong, I. Kim, Y. Oh, S. Jeong, J. Moon, Solar Energy Materials and Solar Cells, Vol.128, pp. 362-3368, (2014); https://doi.org/10.1016/j.solmat.2014.06.013

[4] X. Liang, P. Guo, R. Deng, D. Pan. D. Pan, X. 00Wei, RSC Adv, Vol.4, No.12, pp.5044-5046, (2012); https://doi.org/10.1039/c2ra20198d

[5] Y. Cui, R. Deng, G. Wang, D. Pan, of Materials Chemistry, Vol.22, No.43, pp. 23136-23140, (2012); https://doi.org/10.1039/c2jm33574c

[6] M. Quintero, E. Moreno, S. Alvarez, J. Marquina, C. Rincon, E. Quintero, P. Grima, J. A. Heano, M. A. Macias, Artículo Regular, Vol.34, No.1, pp. 28-38 ,(2014).

[7] A. S. Hassanien, I. M. El Radaf, Physica B: Condensed Matter, Vol.585, pp. 1-24 , (2020); https://doi.org/10.1016/j.physb.2020.412110

[8] G. S. D. Babu, X. S. Shajan, Materials Today, Vol.4, No.14, pp.12592-12599, (2017); https://doi.org/10.1016/j.matpr.2017.10.067

[9] T. Özdal, H. Kavak, Journal of Alloys and Compounds, Vol.725, pp. 644-651, (2017); https://doi.org/10.1016/j.jallcom.2017.07.209

[10] S. Marchionna, A. L. Donne, M. Merlini, S. Binetti, M. Acciarri, F. Cernuschi, Journal of Alloys and Compounds, Vol.693, pp.95-102, (2017); https://doi.org/10.1016/j.jallcom.2016.09.176

[11] L. Chen, H. Deng, J. Tao, W. Zhou, L. Sun, F. Yue, P. Yang, J. Chu, Journal of Alloys and Compounds, Vol.640, pp.1 -23, (2015); https://doi.org/10.1016/j.jallcom.2015.03.225

[12] X. Wang, T. Liu, F. Yu, H. Hou, Optoelectronics and Advanced Materials, Vol.13, pp.7-8, (2019).

[13] J. Yu, H. Deng, L. Chen, J. Tao, Q. Zhang, B. Guo, L. Sun, P. Yang, X. Zhenga, J. Chu, Materials Chemistry and Physics, Vol.211, pp.1-19, (2018); https://doi.org/10.1016/j.matchemphys.2018.03.009

[14] M. A. Ahmed, N. A. Bakr, A. A. Kamil, Chalcogenide Letters, Vol .16, No. 5, pp.231-239, (2019).

[15] C. Kittel, Introduction to Solid State Physics, John Wiley and Sons Inc.8th Edition, (2005).

[16] A. M. Mohammed, M. M. Mohammed, L.A. Hussein, Digest Journal of Nanomaterials and Biostructures, Vol.15, No.1, pp.231-241, (2020).

[17] L. Nie, J. Yang, D. Yang, S. Liu, Journal of Materials Science: Materials in Electronics, Vol.30, No. 4 , pp.3760-3766, (2019); https://doi.org/10.1007/s10854-018-00658-2

[18] L. Chen, H. Deng, J. Tao, H. Cao, L. Sun, P. Yang, J. Chu, Acta Materialia, Vol.109, pp.1-7, (2016); https://doi.org/10.1016/j.actamat.2016.02.057

[19] R. R. Parbhakar, S. Zhenghua, Z. Xin, T. Baikie, L. S. Woei, S. Shukla, S. K. Batabyal, O.Gunawan, L. H. Wong, Solar Energy Materials and Solar Cells, Vol. 157, pp. 867-873, (2016); https://doi.org/10.1016/j.solmat.2016.07.006

[20] N. A. Bakr, N. N. Jandow and N. F. Habubi, International Letters of Chemistry, Physics and Astronomy. Vol. 20, No. 1, pp. 52-63, (2014); https://doi.org/10.18052/www.scipress.com/ILCPA.39.52